APL Materials

RESEARCH ARTICLE | APRIL 18 2025

Suppression of ferromagnetism in rippled $La_{2/3}Sr_{1/3}MnO_3$ membrane with process-induced strain prepared by epitaxial lift-off technique

Kota Kanda; Ryuji Atsumi; Takamasa Usami ; Takumi Yamazaki ; Kohei Ueda ; Takeshi Seki ; Shigeki Miyasaka ; Jobu Matsuno ; Junichi Shiogai

APL Mater. 13, 041117 (2025)
https://doi.org/10.1063/5.0263925

Suppression of ferromagnetism in rippled $La_{2/3}Sr_{1/3}MnO_3$ membrane with process-induced strain prepared by epitaxial lift-off technique

Cite as: APL Mater. 13, 041117 (2025); doi: 10.1063/5.0263925
Submitted: 7 February 2025 • Accepted: 31 March 2025 •
Published Online: 18 April 2025

Kota Kanda,[1] Ryuji Atsumi,[1] Takamasa Usami,[2,3] Takumi Yamazaki,[4] Kohei Ueda,[1,2] Takeshi Seki,[4,5] Shigeki Miyasaka,[6] Jobu Matsuno,[1,2] and Junichi Shiogai[1,2,a)]

AFFILIATIONS

[1] Department of Physics, Osaka University, Toyonaka, Osaka 560-0043, Japan
[2] Division of Spintronics Research Network, Institute for Open and Transdisciplinary Research Initiatives, Osaka University, Suita, Osaka 565-0871, Japan
[3] Center for Spintronics Research Network, Graduate School of Engineering Science, Osaka University, Toyonaka, Osaka 560-8531, Japan
[4] Institute for Materials Research, Tohoku University, Sendai, Miyagi 980-8577, Japan
[5] Center for Science and Innovation in Spintronics, Tohoku University, Sendai, Miyagi 980-8577, Japan
[6] Department of Material Science, Graduate School of Science, University of Hyogo, Ako, Hyogo 678-1297, Japan

[a)] **Author to whom correspondence should be addressed:** junichi.shiogai.sci@osaka-u.ac.jp

ABSTRACT

Transition metal oxides are a platform for exploring strain-engineered intriguing physical properties and developing spintronic or flexible electronic functionalities owing to the strong coupling of spin, charge, and lattice degrees of freedom. In this study, we exemplify the strain-engineered magnetism of $La_{2/3}Sr_{1/3}MnO_3$ in freestanding and rippled membrane forms without and with process-induced strain, respectively, prepared by the epitaxial lift-off technique. We find that the deposition of the Pt/Ti stressor suppresses the crack formation in the lift-off process and induces a ripple structure in the $La_{2/3}Sr_{1/3}MnO_3$ membrane. Laser micrograph and Raman spectroscopy show a ripple period of about 30 μm and a height of a few μm, where alternating convex and concave structures are subjected to a tensile strain of 0.6% and a compressive strain of 0.5%, respectively. While the freestanding $La_{2/3}Sr_{1/3}MnO_3$ membrane exhibits room-temperature ferromagnetism, the macroscopic magnetic transition temperature (T_C) of the rippled membrane is reduced by as much as 27%. Temperature-variable Kerr microscopy observation in the rippled membrane reveals that the spatial variation of T_C is ~4% of the macroscopic T_C, which coincides with the local strains at convex and concave structures. The large reduction of macroscopic T_C in the rippled membrane may be ascribed to the lattice disorders due to the strain gradient. Our demonstration of tuning ferromagnetism by the ripple structure validates the high potential of the process-induced strain in the epitaxial lift-off technique and paves the way for strain-mediated emerging physical properties in various transition metal oxides.

Strain often plays an important role in tuning physical properties in materials with strongly localized electrons, where their spin and charge degrees of freedom are coupled to lattices such as bond lengths and angles, as well as coordination symmetry.[1] In such strongly correlated systems, tuning their magnetic or electronic properties with external and/or internal strains is particularly attractive because it offers a promising platform for magnetostrictive energy harvesting,[2,3] strain gauge application,[4] and the development of other spintronic or flexible electronic functionalities.[5–7] With the aim of the modulation of magnetic properties in such functional materials by strain engineering, an effective approach for strain application is a matter of interest.

One representative example is an epitaxial strain in thin-film growth by selecting proper lattice-mismatched substrates. In the

thin-film approach, manganite perovskites have been intensively studied: modulation of their electron correlation and magnetic ground states has been demonstrated by introducing in-plane tensile or compressive epitaxial strains.[8] However, the large and continuous control of strain is difficult in this approach because the maximum applicable strain is limited to about 3% by the formation of dislocations,[9] and the lattice constant of the available substrate is discrete. Another example is a single or few atomic-layer-thick exfoliated flakes of van der Waals (vdW) magnets prepared on a flexible substrate or in suspended form. In these sample configurations, the magnetic properties can be well controlled by stretching the base substances, as exemplified in the Fe_3GeTe_2 and CrSBr flakes.[10,11] Furthermore, the process-induced strain, in which depositing thin-film stressors transfers their residual strain on the underlayer, has been utilized for lateral imprinting of strain-sensitive physical properties. Although this approach was originally developed for high-performance complementary metal–oxide–semiconductor (CMOS) applications,[12] it has been recently applied to the vdW materials flakes[13,14] owing to its high compatibility with the freestanding nature of the vdW materials and conventional lithography techniques.[15]

Recently, the epitaxial lift-off technique[16] using a water-soluble $Sr_3Al_2O_6$ sacrificial layer has attracted considerable attention[17,18] for the synthesis of freestanding membranes of various transition metal oxides[19–23] and their heterostructures.[17,24] One extreme characteristic of the freestanding membrane is the mechanical robustness against various forms of strain, such as biaxial or uniaxial form with a large stretching of up to 8%,[21] and gradient or bending form.[25] To date, a strain-mediated magnetic phase transition has been demonstrated in various functional magnets with membrane forms, such as a stretched membrane of manganite[21] or rippled membranes of the Heusler compound.[26,27] While the high utility of the process-induced strain is also expected in freestanding membranes of the strongly correlated materials, modulation of their structures and magnetic properties by this approach has not been explicitly demonstrated so far.

A key to the process-induced strain application to membranes is a choice of stressor materials: it should possess internal strain for structural modulation and mechanical robustness for large-area exfoliation in the lift-off process. In this study, by using the Pt/Ti thin-film cap layer as a stressor, we apply the process-induced strain to the membrane of prototypical ferromagnetic transition metal oxide $La_{2/3}Sr_{1/3}MnO_3$, prepared by the epitaxial lift-off technique. We find that crack formation is greatly suppressed with the Pt/Ti cap layer, and the process-induced strain forms a ripple structure in the lift-off process. The induced strain in the rippled membrane drives a magnetic phase transition from ferromagnet to paramagnet at room temperature. Our experimental results suggest a high potential for process-induced strain not only for conventional CMOS technology or vdW materials but also for exploring emergent physical properties of freestanding membranes of strongly correlated materials.

The freestanding membrane of $La_{2/3}Sr_{1/2}MnO_3$ was obtained by the epitaxial lift-off technique from a thin-film heterostructure of a 60-nm-thick $La_{2/3}Sr_{1/2}MnO_3$ layer and a 17-nm-thick $Sr_3Al_2O_6$ sacrificial layer prepared on a $SrTiO_3$(001) substrate by pulsed-laser deposition. As depicted in Fig. 1(a), the $La_{2/3}Sr_{1/2}MnO_3$ film [bulk lattice constant a_{LSMO} = 3.894 Å (Ref. 28)] is subjected to the tensile strain from the $Sr_3Al_2O_6$ underlayer ($a_{SAO}/4$ = 3.961 Å). By dipping the heterostructure in distilled water, the $Sr_3Al_2O_6$ sacrificial layer was dissolved, and the tensile strain in the $La_{2/3}Sr_{1/2}MnO_3$ layer was fully released, as previously reported.[23] Concomitantly, a significant number of cracks with their typical lateral size of ~10 μm were randomly distributed in the released $La_{2/3}Sr_{1/2}MnO_3$ membrane, as shown in the micrograph [Fig. 1(b)].

This situation is drastically changed when depositing a 100-nm-thick Pt/10-nm-thick Ti cap layer on the $La_{2/3}Sr_{1/2}MnO_3$ layer prior to etching the sacrificial layer [Fig. 1(c)]. Figure 1(d) shows the top view micrograph of the Pt/Ti/$La_{2/3}Sr_{1/2}MnO_3$ membrane. Here, the micrograph was taken from the $La_{2/3}Sr_{1/2}MnO_3$ layer. After the etching, the formation of the cracks was strongly suppressed, and a large, continuous rippled membrane with a lateral size of the order of mm was obtained [Fig. 1(e)]. Note that the directions of rippled edges

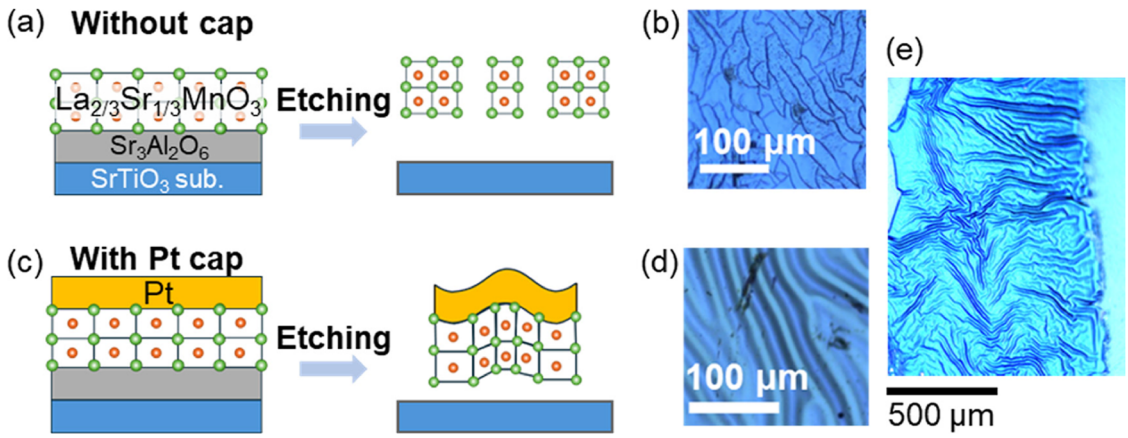

FIG. 1. (a) Procedure of epitaxial lift-off technique for the $La_{2/3}Sr_{1/2}MnO_3/Sr_3Al_2O_6$ heterostructure accompanied by epitaxial strain relaxation and crack formation. (b) Top-view micrograph of the freestanding $La_{2/3}Sr_{1/2}MnO_3$ membrane. (c) Formation of ripple structure in the lift-off process for the Pt/Ti capped $La_{2/3}Sr_{1/2}MnO_3$ membrane. (d) Top-view micrograph of the rippled Pt/Ti/$La_{2/3}Sr_{1/2}MnO_3$ membrane taken from the $La_{2/3}Sr_{1/2}MnO_3$ face. (e) A wide view of (d) showing mm-scale crack-free membrane with ripple structure.

are not well aligned. We consider that the strong adhesive property of the Ti layer between the top Pt layer and the bottom oxide layer plays a crucial role in the $La_{2/3}Sr_{1/2}MnO_3$ layer being released on the mm scale.[29] The analysis of the x-ray diffraction patterns (see Fig. S1 of the supplementary material) indicates that the Pt layer is subjected to 0.75% compressive strain in the plane and 2% tensile strain out of the plane. According to our previous report,[23] on the other hand, the $La_{2/3}Sr_{1/2}MnO_3$ layer is subjected to 2.1% tensile strain in the plane at the interface with the $Sr_3Al_2O_6$ layer and fully relaxed at around 16 nm apart from the interface. We speculate that the transferring of the compressive strain of the Pt stressor on the relaxed top surface of the $La_{2/3}Sr_{1/2}MnO_3$ layer and the relaxation of tensile strain in the strained bottom surface of the $La_{2/3}Sr_{1/2}MnO_3$ layer drive the formation of the ripple structure during the releasing process.

To deepen the understanding of the detailed structure of the rippled membrane, laser microscopy and Raman spectroscopy were carried out for height and strain profiles, respectively. Figure 2(a) shows a two-dimensional height profile of a typical area of the rippled membrane. Apparently, the rippled membrane possesses convex and concave structures with a period of tens of μm in the plane and a height of a few μm [see also the one-dimensional height profile along the white dashed line in the bottom image of Fig. 2(a)]. Here, the strain ε in the convex and concave parts of the rippled membrane composed of three layers is estimated by the relation[30,31]

$$\varepsilon = \frac{1}{R}\frac{\sum_{i=1}^{3} E_i t_i \left[\left(\sum_{i=1}^{3} t_i\right) - \frac{t_i}{2}\right]}{\sum_{i=1}^{3} E_i t_i},$$

where R is a radius of the curvature when we regard the bent $La_{2/3}Sr_{1/2}MnO_3$ layer surface as a circular sector [see the inset of Fig. 2(c)], E_i and t_i represent Young's modulus[32] and the thickness of the i-th layer, respectively. The averaged values of ε are calculated to be +0.6% and −0.5% at convex and concave structures, respectively, along the white line in Fig. 2(a). Figure 2(b) shows Raman

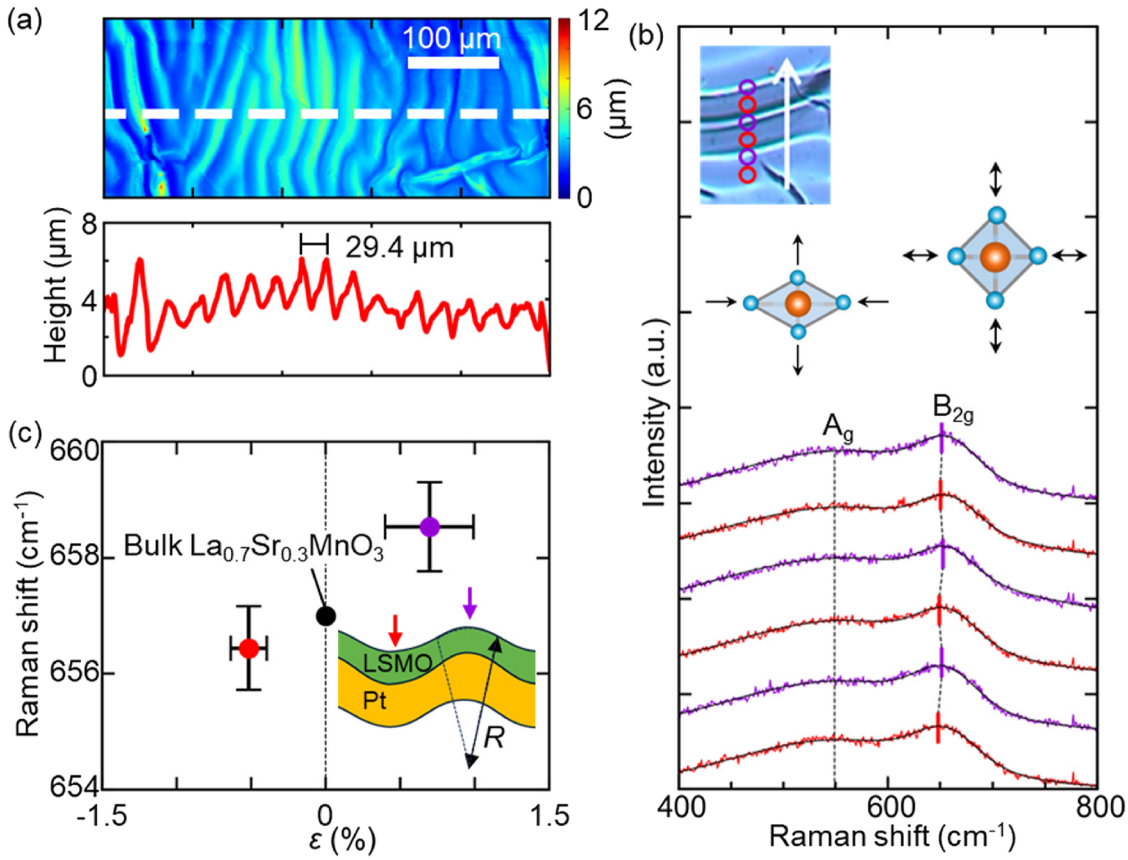

FIG. 2. (a) Laser micrograph of the rippled $La_{2/3}Sr_{1/2}MnO_3$ membrane. (Top) Color plot of areal height profile and (bottom) line profile along the white dashed line. (b) Raman spectrum measured at convex (purple) and concave (red) structures. For clarity, the background is subtracted. Solid black lines indicate the analysis of Gaussian fitting, and vertical red and purple segments around the B_{2g} peak indicate the extracted peak positions. (Inset) Top view photograph of the measurement area. (c) Averaged values of the Raman shift for convex (purple) and concave (red) structures as well as that of the powder $La_{0.7}Sr_{0.3}MnO_3$ sample reported previously (black).[33] Vertical and horizontal error bars correspond to the variation in cross-sectional curvatures and Raman shifts among investigated points, respectively. (Inset) Schematic of a cross-sectional view of ripple structures.

spectra obtained at the convex (purple circles in the inset) and concave (red) parts of the ripple structure after the background signal is subtracted. Note that the spot diameter of the present spectrometer is 15 μm, which is small enough to capture the properties specific to the convex and concave structures. As can be seen, two broad Raman peaks were observed around 540 and 650 cm^{-1}, which we assigned to the A_g (Jahn–Teller mode) and B_{2g} (breathing mode) phonons, respectively.[33] The characteristic Raman spectra corresponding to the Jahn–Teller mode obtained at convex and concave structures do not show a detectable difference, indicating that the impact of the ripple structure is insignificant on the out-of-phase vibration of Mn–O–Mn bonding of MnO_6 octahedrons. Figure 2(c) shows the relation of Raman shifts obtained by B_{2g} phonons [red and purple vertical segments in Fig. 2(b)] and strain estimated by line profile [Fig. 2(a)] for convex (purple circle) and concave (red circle), as well as that in $La_{0.7}Sr_{0.3}MnO_3$ powder reported in previous work (black circle).[33] In contrast to the insensitive A_g peak, we observe a slight shift of the B_{2g} peak of breathing mode: the characteristic wave number for the convex (concave) structure is shifted lower (higher). The breathing mode corresponds to the in-phase vibration of Mn–O–Mn bonding of MnO_6 octahedrons, which is directly related to the average length of Mn–O–Mn bonding. For previous powder experiments,[33] the compressive strain by chemical doping exhibits the red shift with respect to the non-doped $La_{0.7}Sr_{0.3}MnO_3$, which is qualitatively consistent with our estimation shown in Fig. 2(c). From these observations, we conclude that the bending strain in the convex and concave structure modulates the Mn–Mn bonding distance more effectively than the Jahn–Teller strain.

The impact of the ripple structure on magnetic properties was first characterized by the magnetic field (H) dependence of magnetization [$M(H)$ curve] of the freestanding and rippled $La_{2/3}Sr_{1/3}MnO_3$ membranes when H was applied in the sample plane. Figures 3(a) and 3(b) show those $M(H)$ curves measured at T = 300 K. The fully relaxed freestanding membrane exhibits ferromagnetism with a good squareness, being consistent with the room-temperature ferromagnetism of $La_{2/3}Sr_{1/3}MnO_3$[34] and our previous report.[23] In stark contrast, the rippled membrane does not show detectable magnetization at T = 300 K. Note that such a large reduction of the magnetization was not detected before the epitaxial lift-off process, as shown in Fig. S2 of the supplementary material. Figures 3(c) and 3(d) show the set of $M(H)$ curves measured at T = 5 K. The $M(H)$ curves for the freestanding and rippled membranes fully saturate in the magnetic field range of 0.6 and 0.5 T, respectively. The obtained value of saturation magnetization is 3.42 μ_B/Mn for the freestanding membrane [Fig. 3(c)], close to the ideal value of 3.67 μ_B/Mn (μ_B: Bohr magneton) under the assumption of the mixed valence of Mn^{3+} and Mn^{4+} ions in the stoichiometric $La_{2/3}Sr_{1/3}MnO_3$. This consistency also suggests the fully relaxed nature of the freestanding membrane. On the other hand, the saturation magnetization is only 2.02 μ_B/Mn for the rippled membrane, as shown in Fig. 3(d).

Such sharp differences in the magnetization between the freestanding and rippled membranes are more clearly seen in the temperature (T) dependence of magnetization [$M(T)$ curve] shown in

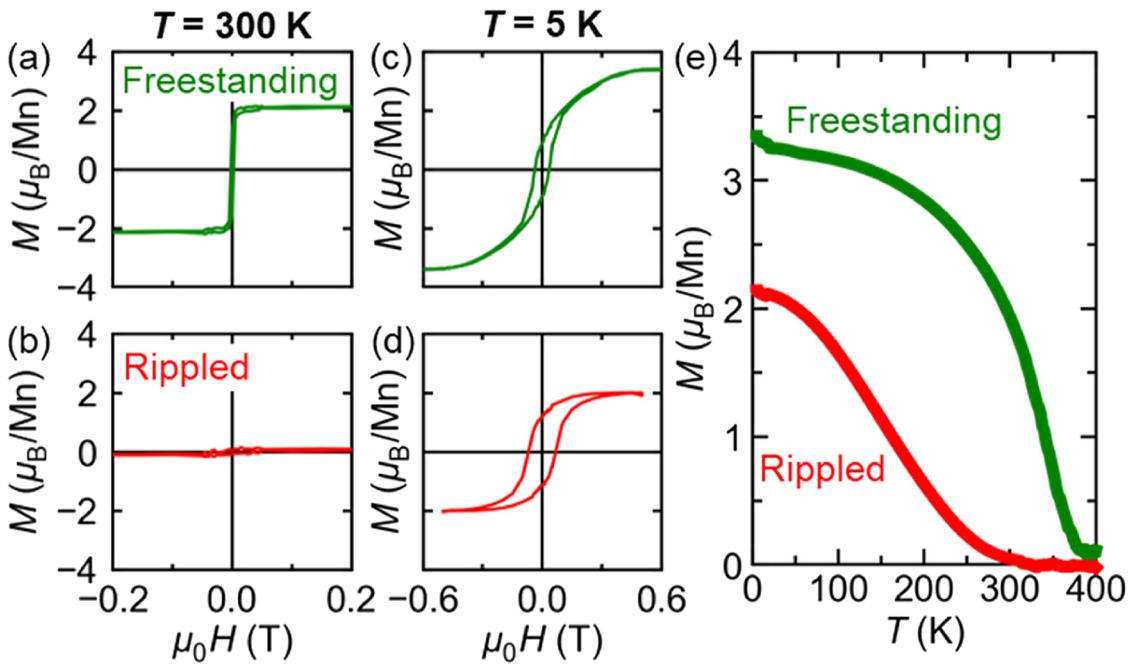

FIG. 3. In-plane magnetic hysteresis loops for (a) freestanding and (b) rippled $La_{2/3}Sr_{1/3}MnO_3$ membranes measured at T = 300 K and those for (c) freestanding and (d) rippled membranes measured at T = 5 K. (e) Temperature dependence of magnetization $M(T)$ for freestanding (green) and rippled (red) membranes. Measurements were performed at an in-plane field of $\mu_0 H$ = 1.5 T for the freestanding membrane and at $\mu_0 H$ = 0.5 T for the rippled membrane.

Fig. 3(e). As expected by the development of the ferromagnetism at T = 300 K for the freestanding membrane [Fig. 3(a)], the $M(T)$ curves exhibit a high ferromagnetic transition temperature T_C around T = 370 K, well above room temperature. On the other hand, T_C for the rippled membrane is strongly suppressed, where $M(T)$ starts to develop around 270 K and reaches about 2 μ_B/Mn at the lowest temperature. By comparing to the fully magnetized state in the freestanding membrane, it is suggested that the local structural variation, i.e., the tensile and compressive strain in the convex and concave structure, respectively, reduces T_C by 27% and saturation magnetization in the rippled membrane.

To clarify the correlation between ripple structure and magnetism, we performed Kerr microscopy measurements with descending temperature. Figure 4(a) shows the raw image of reflection contrast in the rippled membrane. The bright contrast corresponds to alternating convex (purple arrows) and concave (red arrows) structures. The reflection from the area between convex and concave structures was not clearly detected because the $La_{2/3}Sr_{1/3}MnO_3$ surface is tilted from the normal to the sample stage. Although the convex and concave structures show almost the same brightness, the height profile was judged by defocusing while moving the sample stage along the z-axis. To extract only the contribution sensitive to the magnetization, we calculate a subtraction of the raw image taken at $\mu_0 H$ = −0.1 T from that at $\mu_0 H$ = +0.1 T. Figure 4(b) shows a differential image taken at T = 290 K, where no bright contrast is detected because the ferromagnetism is not well developed at this temperature. At T = 280 K, weak contrast starts to emerge along both convex and concave structures [Fig. 4(c)]. Below T = 270 K, the white lines in the concave are slightly brighter than those in the convex structure [Fig. 4(d)], and both contrasts become comparable at T = 260 K [Fig. 4(e)]. Such temperature variation of brightness is linked to the development of ferromagnetism in the $M(T)$ curve around T = 270 K. From these results, we conclude that the spatial variation of local T_C by local strain at the convex and concave structures is ~10 K, which corresponds to 4% with respect to macroscopic T_C of 270 K.

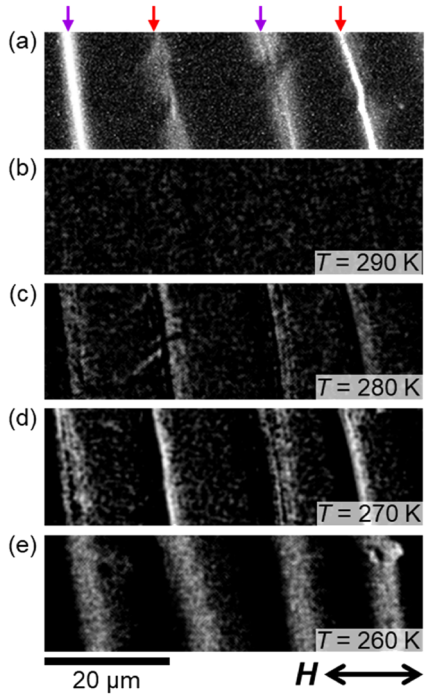

FIG. 4. (a) Reflectivity image obtained by Kerr microscopy. (b)–(e) The contrast difference of reflectivity images between at $\mu_0 H$ = + 0.1 T and −0.1 T, obtained at T = (b) 290, (c) 280, (d) 270, and (e) 260 K. Purple and red arrows indicate the convex and concave structures, respectively. A horizontal arrow indicates the direction of H.

Finally, we quantitatively discuss the relation between local structure and magnetization. For ABO_3-type perovskites, the strength of p–d hybridization and, thus, T_C depends on both the B–O–B bond angle θ_{B-O-B} and the bond length d_{B-O} (where B = Mn in manganites).[35] Judging from the A_g mode insensitive to the ripple structure as shown in Fig. 2, we can assume that the Mn–O–Mn bond angle is independent of the tensile or compressive strain in the present ripple structure. Based on the tight binding approximation, the pd hybridization $t_{p\text{-}d}$ between Mn and O atoms is proportional to $1/d_{Mn-O}^{7/2}$ (Ref. 35). Since the Mn ions are well separated from each other, the effective d–d interaction t_{d-d} via the O ion is the square of $t_{p\text{-}d}$ (Ref. 36). Therefore, from the naïve expectation of T_C being proportional to t_{d-d} and the assumption of $\theta_{Mn-O-Mn}$ being constant, the modulation of T_C by strain between convex and concave structures ($\Delta\varepsilon \sim 1.1\%$) is estimated as $\Delta T_C/T_C \sim 7\Delta\varepsilon \sim 8\%$. This difference is in the same order as the spatial variation of local T_C revealed in the results of the Kerr micrography (Fig. 4). In contrast, the reduction of macroscopic T_C in the rippled membrane from the freestanding membrane is about 27%, much larger than that from our estimation. Therefore, we ascribe this discrepancy to the role of the strain gradient in the rippled membrane. One possible explanation related to the strain gradient is a quenched disorder[37] from the averaged structure or freestanding form. According to the Monte Carlo simulation performed for the optimally doped ferromagnetic manganites,[38–40] it has been demonstrated that the quenched disorder enhances electron–phonon coupling, which suppresses the electron hopping probability and induces metal-to-insulator transition. Because of the strong coupling between electrical transport and magnetism in manganites, the enhanced quenched disorder is also related to the suppression of ferromagnetic order in the present rippled membrane. Another possibility of T_C modulation related to the strain gradient may be the effect of strain-mediated off-stoichiometry.[41,42] Further characterization of the microscopic structure, numerical analysis of strain distribution, and measurement of electrical transport properties are needed for more quantitative discussion.

In summary, we showed that the use of a Pt/Ti layer as a stressor can suppress the crack formation and apply the process-induced strain into the $La_{2/3}Sr_{1/3}MnO_3$ membrane prepared by the epitaxial lift-off technique, which resulted in the formation of a ripple structure. The induced strain and strain gradient in the rippled membrane effectively affect the Mn–O bonding length, which allows us to modulate magnetic phases at room temperature. Considering the compatibility of process-induced strain to conventional lithography techniques, our proof-of-concept study in the application of this approach to the manganite membrane can be

extended to artificial lateral patterning of the strain and strain gradient on two-dimensional membranes of various strongly correlated materials.

The supplementary material is available for structural characterization using x-ray diffraction patterns.

The authors acknowledge Kohei Hamaya at Osaka University for Kerr microscopy, Makoto Kohda at Tohoku University for laser microscopy, and Jason K. Kawasaki at the University of Wisconsin-Madison for stimulating discussion. This work was partly performed under the GIMRT Program of the Institute for Materials Research, Tohoku University (Proposal No. 202212-CRKEQ-0007). The Raman experiment was performed using an NRS-3100T spectrometer (JASCO Co., Ltd.) with the help of Takashi Harada at the Research Center for Solar Energy Chemistry, Graduate School of Engineering Science, Osaka University. This work was supported by JST, PRESTO Grant No. JPMJPR21A8, and JSPS, KAKENHI Grant Nos. JP22K18894 and JP23K26379, and the Iketani Science and Technology Foundation and the Tanikawa Foundation.

AUTHOR DECLARATIONS

Conflict of Interest

The authors have no conflicts to disclose.

Author Contributions

K.K. and R.A. contributed equally to this work.

Kota Kanda: Data curation (equal); Formal analysis (equal); Visualization (equal); Writing – original draft (equal). **Ryuji Atsumi**: Data curation (equal); Formal analysis (equal); Visualization (equal); Writing – original draft (equal). **Takamasa Usami**: Data curation (equal); Formal analysis (equal); Resources (equal); Writing – review & editing (equal). **Takumi Yamazaki**: Resources (equal); Writing – review & editing (equal). **Kohei Ueda**: Writing – review & editing (equal). **Takeshi Seki**: Resources (equal); Writing – review & editing (equal). **Shigeki Miyasaka**: Formal analysis (equal); Writing – review & editing (equal). **Jobu Matsuno**: Supervision (lead); Writing – review & editing (equal). **Junichi Shiogai**: Conceptualization (lead); Writing – original draft (equal).

DATA AVAILABILITY

The data that support the findings of this study are available from the corresponding authors upon reasonable request.

REFERENCES

[1] Y. Tokura, "Critical features of colossal magnetoresistive manganites," Rep. Prog. Phys. **69**, 797 (2006).
[2] F. Narita and M. Fox, "A review on piezoelectric, magnetostrictive, and magnetoelectric materials and device technologies for energy harvesting applications," Adv. Eng. Mater. **20**, 1700743 (2018).
[3] L. Wang and F. G. Yuan, "Vibration energy harvesting by magnetostrictive material," Smart Mater. Struct. **17**, 045009 (2008).
[4] M. Löhndorf, T. Duenas, M. Tewes, E. Quandt, M. Rührig, and J. Wecker, "Highly sensitive strain sensors based on magnetic tunneling junctions," Appl. Phys. Lett. **81**, 313 (2002).
[5] J. Huang, H. Wang, X. Sun, X. Zhang, and H. Wang, "Multifunctional $La_{0.67}Sr_{0.33}MnO_3$ (LSMO) thin films integrated on mica substrates toward flexible spintronics and electronics," ACS Appl. Mater. Interfaces **10**, 42698 (2018).
[6] T. Vemulkar, R. Mansell, A. Fernández-Pacheco, and R. P. Cowburn, "Toward flexible spintronics: Perpendicularly magnetized synthetic antiferromagnetic thin films and nanowires on polyimide substrates," Adv. Funct. Mater. **26**, 4704 (2016).
[7] A. Bedoya-Pinto, M. Donolato, M. Gobbi, L. E. Hueso, and P. Vavassori, "Flexible spintronic devices on Kapton," Appl. Phys. Lett. **104**, 062412 (2014).
[8] Y. Konishi, Z. Fang, M. Izumi, T. Manako, M. Kasai, H. Kuwahara, M. Kawasaki, K. Terakura, and Y. Tokura, "Orbital-state-mediated phase-control of manganites," J. Phys. Soc. Jpn. **68**, 3790 (1999).
[9] J. C. Bean, L. C. Feldman, A. T. Fiory, S. Nakahara, and I. K. Robinson, "Ge_xSi_{1-x}/Si strained-layer superlattice grown by molecular beam epitaxy," J. Vac. Sci. Technol. A **2**, 436 (1984).
[10] Y. Wang, C. Wang, S. J. Liang, Z. Ma, K. Xu, X. Liu, L. Zhang, A. S. Admasu, S. W. Cheong, L. Wang, M. Chen, Z. Liu, B. Cheng, W. Ji, and F. Miao, "Strain-sensitive magnetization reversal of a van der Waals magnet," Adv. Mater. **32**, 2004533 (2020).
[11] J. Cenker, S. Sivakumar, K. Xie, A. Miller, P. Thijssen, Z. Liu, A. Dismukes, J. Fonseca, E. Anderson, X. Zhu, X. Roy, D. Xiao, J. H. Chu, T. Cao, and X. Xu, "Reversible strain-induced magnetic phase transition in a van der Waals magnet," Nat. Nanotechnol. **17**, 256 (2022).
[12] S. E. Thompson *et al.*, "A 90-nm logic technology featuring strained-silicon," IEEE Trans. Electron Devices **51**, 1790 (2004).
[13] T. Peña, A. Dey, S. A. Chowdhury, A. Azizimanesh, W. Hou, A. Sewaket, C. Watson, H. Askari, and S. M. Wu, "Moiré engineering in 2D heterostructures with process-induced strain," Appl. Phys. Lett. **122**, 143101 (2023).
[14] Y. Zhang, H. L. Zhao, S. Huang, M. A. Hossain, and A. M. van der Zande, "Enhancing carrier mobility in monolayer MoS_2 transistors with process-induced strain," ACS Nano **18**, 12377 (2024).
[15] Y. Zhang, M. A. Hossain, K. J. Hwang, P. F. Ferrari, J. Maduzia, T. Peña, S. M. Wu, E. Ertekin, and A. M. van der Zande, "Patternable process-induced strain in 2D monolayers and heterobilayers," ACS Nano **18**, 4205 (2024).
[16] P. Demeester, I. Pollentier, P. D. Dobbelaere, C. Brys, and P. V. Daele, "Epitaxial lift-off and its applications," Semicond. Sci. Technol. **8**, 1124 (1993).
[17] D. Lu, D. J. Baek, S. S. Hong, L. F. Kourkoutis, Y. Hikita, and H. Y. Hwang, "Synthesis of freestanding single-crystal perovskite films and heterostructures by etching of sacrificial water-soluble layers," Nat. Mater. **15**, 1255 (2016).
[18] F. M. Chiabrera, S. Yun, Y. Li, R. T. Dahm, H. Zhang, C. K. R. Kirchert, D. V. Christensen, F. Trier, T. S. Jespersen, and N. Pryds, "Freestanding perovskite oxide films: Synthesis, challenges, and properties," Ann. Phys. **534**, 2200084 (2022).
[19] G. Dong *et al.*, "Super-elastic ferroelectric single-crystal membrane with continuous electric dipole rotation," Science **366**, 475 (2019).
[20] Z. Chen, B. Y. Wang, B. H. Goodge, D. Lu, S. S. Hong, D. Li, L. F. Kourkoutis, Y. Hikita, and H. Y. Hwang, "Freestanding crystalline $YBa_2Cu_3O_{7-x}$ heterostructure membranes," Phys. Rev. Mater. **3**, 060801(R) (2019).
[21] S. S. Hong, M. Gu, M. Verma, V. Harbola, B. Y. Wang, D. Lu, A. Vailionis, Y. Hikita, R. Pentcheva, J. M. Rondinelli, and H. Y. Hwang, "Extreme tensile strain states in $La_{0.7}Ca_{0.3}MnO_3$ membranes," Science **368**, 71 (2020).
[22] P. T. P. Le, J. E. ten Elshof, and G. Koster, "Epitaxial lift-off of freestanding (011) and (111) $SrRuO_3$ thin films using a water sacrificial layer," Sci. Rep. **11**, 12435 (2021).
[23] R. Atsumi, J. Shiogai, T. Yamazaki, T. Seki, K. Ueda, and J. Matsuno, "Impact of epitaxial strain relaxation on ferromagnetism in a freestanding $La_{2/3}Sr_{1/3}MnO_3$ membrane," Jpn. J. Appl. Phys. **62**, 100902 (2023).
[24] J. Shiogai and A. Tsukazaki, "Superconducting FeSe membrane synthesized by etching of water-soluble $Sr_3Al_2O_6$ layer," Appl. Phys. Lett. **122**, 052602 (2023).
[25] L. Han, G. Dong, M. Liu, and Y. Nie, "Freestanding perovskite oxide membranes: A new playground for novel ferroic properties and applications," Adv. Funct. Mater. **34**, 2309543 (2024).
[26] D. Du, S. Manzo, C. Zhang, V. Saraswat, K. T. Genser, K. M. Rabe, P. M. Voyles, M. S. Arnold, and J. K. Kawasaki, "Epitaxy, exfoliation, and strain-induced magnetism in rippled Heusler membranes," Nat. Commun. **12**, 2494 (2021).

[27]D. Du, J. Hu, and J. K. Kawasaki, "Strain and strain gradient engineering in membranes of quantum materials," Appl. Phys. Lett. **122**, 170501 (2023).
[28]A. Vailionis, H. Boschker, W. Siemons, E. P. Houwman, D. H. A. Blank, G. Rijnders, and G. Koster, "Misfit strain accommodation in epitaxial ABO_3 perovskites: Lattice rotations and lattice modulations," Phys. Rev. B **83**, 064101 (2011).
[29]F. Liu, W. Wu, Y. Bai, S. H. Chae, Q. Li, J. Wang, J. Hone, and X. Y. Zhu, "Disassembling 2D van der Waals crystals into macroscopic monolayers and reassembling into artificial lattices," Science **367**, 903 (2020).
[30]Z. Suo, E. Y. Ma, H. Gleskova, and S. Wagner, "Mechanics of rollable and foldable film-on-foil electronics," Appl. Phys. Lett. **74**, 1177 (1999).
[31]L. Mao, Q. Meng, A. Ahmad, and Z. Wei, "Mechanical analyses and structural design requirements for flexible energy storage devices," Adv. Energy Mater. **7**, 1700535 (2017).
[32]P. Kulandaivelu, K. Sakthipandi, P. Senthil Kumar, and V. Rajendran, "Mechanical properties of bulk and nanostructured $La_{0.61}Sr_{0.39}MnO_3$ perovskite manganite materials," J. Phys. Chem. Solids **74**, 205 (2013).
[33]J. Fan, L. Xu, X. Zhang, Y. Shi, W. Zhang, Y. Zhu, B. Gao, B. Hong, L. Zhang, W. Tong, L. Pi, and Y. Zhang, "Effect of A-site average radius and cation disorder on magnetism and electronic properties in manganite $La_{0.6}A_{0.1}Sr_{0.3}MnO_3$ (A = Sm, Dy, Er)," J. Mater. Sci. **50**, 2130 (2015).
[34]A. M. Haghiri-Gosnet and J. P. Renard, "CMR manganites: Physics, thin films and devices," J. Phys. D: Appl. Phys. **36**, R127 (2003).
[35]W. Harrison, *Electronic Structure and the Properties of Solids: Physics of the Chemical Bond* (Freeman, San Francisco, 1980), Sec. 20 E.
[36]A. J. Millis, T. Darling, and A. Migliori, "Quantifying strain dependence in "colossal" magnetoresistance manganites," J. Appl. Phys. **83**, 1588 (1998).
[37]Y. Tomioka and Y. Tokura, "Global phase diagram of perovskite manganites in the plane of quenched disorder vs one-electron bandwidth," Phys. Rev. B **70**, 014432 (2004).
[38]C. Şen, G. Alvarez, H. Aliaga, and E. Dagotto, "Colossal magnetoresistance observed in Monte Carlo simulations of the one- and two-orbital models for manganites," Phys. Rev. B **73**, 224441 (2006).
[39]S. Kumar and P. Majumdar, "Insulator-metal phase diagram of the optimally doped manganites from the disordered holstein-double exchange model," Phys. Rev. Lett. **96**, 016602 (2006).
[40]C. Şen, G. Alvarez, and E. Dagotto, "Competing ferromagnetic and charge-ordered states in models for manganites: The origin of the colossal magnetoresistance effect," Phys. Rev. Lett. **98**, 127202 (2007).
[41]C. Becher, L. Maurel, U. Aschauer, M. Lilienblum, C. Magén, D. Meier, E. Langenberg, M. Trassin, J. Blasco, I. P. Krug, P. A. Algarabel, N. A. Spaldin, J. A. Pardo, and M. Fiebig, "Strain-induced coupling of electrical polarization and structural defects in $SrMnO_3$ films," Nat. Nanotechnol. **10**, 661 (2015).
[42]A. Herklotz, D. Lee, E. J. Guo, T. L. Meyer, J. R. Petrie, and H. N. Lee, "Strain coupling of oxygen non-stoichiometry in perovskite thin films," J. Phys.: Condens. Matter **29**, 493001 (2017).